FIRST RESULTS FROM THE CHARA ARRAY. IV. THE INTERFEROMETRIC RADII OF LOW-MASS STARS

D. H. BERGER[1]

CHARA Array, Mount Wilson Observatory, Mount Wilson, CA 91023; berger@chara-array.org

D. R. GIES AND H. A. MCALISTER

Center for High Angular Resolution Astronomy, Georgia State University, P.O. Box 3969, Atlanta, GA 30302-3969;
gies@chara.gsu.edu, hal@chara.gsu.edu

T. A. TEN BRUMMELAAR

CHARA Array, Mount Wilson Observatory, Mount Wilson, CA 91023; theo@chara-array.org

T. J. HENRY

Center for High Angular Resolution Astronomy, Georgia State University, P.O. Box 3969, Atlanta,
GA 30302-3969; thenry@chara.gsu.edu

J. STURMANN, L. STURMANN, AND N. H. TURNER

CHARA Array, Mount Wilson Observatory, Mount Wilson, CA 91023;
judit@chara-array.org, sturmann@chara-array.org, nils@chara-array.org

S. T. RIDGWAY AND J. P. AUFDENBERG

National Optical Astronomy Observatory, P.O. Box 26732, Tucson, AZ 85726;
ridgway@noao.edu, jasona@noao.edu

AND

A. MÉRAND

LESIA, UMR8109, Observatoire de Paris-Meudon, 5 place Jules Janssen,
92195 Meudon Cedex, France; antoine.merand@obspm.fr

ABSTRACT

We have measured the angular diameters of six M dwarfs with the CHARA Array, a long-baseline optical interferometer located at Mount Wilson Observatory. Spectral types range from M1.0 V to M3.0 V and linear radii from 0.38 to 0.69 $R_\odot$. These results are consistent with the seven other M dwarf radii measurements from optical interferometry and with those for 14 stars in eclipsing binary systems. We compare all directly measured M dwarf radii to model predictions and find that current models underestimate the true stellar radii by up to 15%–20%. The differences are small among the metal-poor stars but become significantly larger with increasing metallicity. This suggests that theoretical models for low-mass stars may be missing some opacity source that alters the computed stellar radii.

Subject headings: infrared: stars — instrumentation: high angular resolution — instrumentation: interferometers — stars: individual (GJ 15A, GJ 514, GJ 526, GJ 687, GJ 752A, GJ 880) — stars: late-type

1. INTRODUCTION

Cool, low-mass stars dominate the stellar census (Henry et al. 1997; Reid et al. 2004), yet they remain elusive and enigmatic objects. Because of their small size and cool surface temperature, nearby members of our solar neighborhood are still being discovered via proper motion surveys (Hambly et al. 2004; Lépine 2005; Subasavage et al. 2005), and parallaxes are being determined for these new stellar neighbors (Jao et al. 2005; Costa et al. 2005). Furthermore, the low-mass stars we do know about are not well understood. Their fundamental properties are difficult to measure and do not adequately constrain atmospheric and interior stellar models. In addition to effective temperature and mass, the size of field stars at the cool end of the main sequence is arguably one of the most difficult properties to determine.

There are currently only two methods to measure the stellar radii of cool dwarfs directly: light-curve and radial velocity studies of double-lined eclipsing binaries and long-baseline interferometry of single stars. The former method is biased toward main-sequence stars larger than the Sun (Andersen 1991) and the latter toward brighter and larger giants and supergiants. Within the past 10 years, cooler and smaller stars are being added to the database of stars with known fundamental properties. There are 14 known M dwarfs that are members of eclipsing binaries for which we have stellar radii: both components of CM Dra (Lacy 1977; Metcalfe et al. 1996), both components of CU Cnc (Ribas 2003), both components of YY Gem and one component of V818 Tau (Torres & Ribas 2002), both components of BW3 V38 (Maceroni & Montalbán 2004), one component of RX J2130.6+4710 (Maxted et al. 2004), both components of TrES-Her0-07621 (Creevey et al. 2005), and both components of GU Boo (López-Morales & Ribas 2005). From long-baseline optical interferometry, the situation is more bleak as there were heretofore only seven M dwarfs (GJ 15A, GJ 191, GJ 205, GJ 411, GJ 551, GJ 699, and GJ 997) for which stellar radii have been measured (Lane et al. 2001; Ségransan et al. 2003).

Here we report on measurements of the angular diameters of six M dwarfs. We obtained these measurements from observations

[1] Current address: University of Michigan, Department of Astronomy, 500 Church Street, 917 Dennison Building, Ann Arbor, MI 48109-1042.

TABLE 1
Observations

GJ (1)	LHS (2)	Calibrator Name (3)	Baseline (length) (4)	Date (UT) (5)	Number of Observations (6)
15A..........................	3	HD 2952	W1/E1 (314 m)	2004 Oct 9	2
514..........................	352	HD 119550	S1/E1 (331 m)	2004 Jun 11	4
				2004 Jun 12	4
				2004 Jun 14	6
526..........................	47	HD 119550	S1/E1 (331 m)	2004 Jun 6	3
				2004 Jun 7	1
				2004 Jun 8	1
				2004 Jun 13	5
687..........................	450	HD 151541	S1/E1 (331 m)	2004 Jun 26	5
752A........................	473	HD 182101	S1/E1 (331 m)	2004 Jun 5	2
				2004 Jun 6	4
				2004 Jun 8	2
				2004 Jun 11	7
				2004 Jun 12	3
				2004 Jun 13	10
				2004 Jun 14	8
880..........................	533	HD 218261	S2/W1 (249 m)	2003 Dec 16	5

made with the Center for High Angular Resolution Astronomy (CHARA) Array, a six-element optical/near-infrared interferometer located at Mount Wilson Observatory, California. From these measurements, we deduce the linear sizes and further refine the mass-radius relation. In addition, we calculate their surface gravities and effective temperatures. This paper is the fourth in a series of commissioning science observations with the CHARA Array. The other three papers vary in topic from the rapid rotators Regulus (McAlister et al. 2005) and Alderamin (van Belle et al. 2006) to an overview of the CHARA Array (ten Brummelaar et al. 2005).

2. OBSERVATIONS

The majority of observations were completed in 2004 June, while others were mixed into the standard queue observing throughout the end of 2003 and most of 2004. All observations were made using the K' filter ($\lambda_0 = 2.13$ μm, $\Delta\lambda = 0.35$ μm; note that the central wavelength for the filter alone differs slightly from the system effective wavelength adopted by McAlister et al. [2005], but the difference has a negligible effect on our results). Data for GJ 15A were obtained using the most western and eastern telescopes (W1 and E1, respectively) and for GJ 880 using the inner southern telescope (S2) and W1. The data for the remaining targets were observed with the most southern telescope (S1) and E1. The maximum baseline separations between these telescopes are 314 m for W1-E1, 249 m for S2-W1, and 331 m for S1-E1. In these configurations, angular diameters as small as 0.5 mas can readily be measured at the K' spectral band.

Targets were chosen from the Gliese & Jahreiß (1991) catalog based on color ($B - V > 1$) and distance (parallax $\pi > 100$ mas) such that their predicted angular size exceeded 0.4 mas. Targets also had to be within the detection limits of the instrument ($B < 11$ for tip-tilt correction, $V < 10$ for image acquisition, and $K' < 6$ for the near-IR detector). Table 1 is a summary of the observations for this paper. Column (1) is the Gliese & Jahreiß catalog designation, column (2) is the Luyten Half-Second (LHS) catalog designation (Luyten 1979), column (3) gives the name of the calibrator star, column (4) indicates the telescope pair

(and baseline) used, column (5) gives the UT observation date, and column (6) gives the number of observations.

Measurements of all but GJ 15A were taken using the "CHARA Classic" beam combiner. It is a two-beam, pupil-plane (or Michelson) combiner utilizing path length modulation; details of the instrumentation and configuration are given by Sturmann et al. (2003). GJ 15A was observed with FLUOR, a single-mode fiber beam combiner designed by collaborators at the Paris Observatory (Coudé du Foresto et al. 2003), because it was the available instrument at the time and the target was within its sensitivity limits. The calibrator for GJ 15A was HD 2952 and was chosen from the "Calibrator Stars for 200 m Baseline Interferometry"[2] catalog (Mérand et al. 2005), which includes corrections for limb darkening. While FLUOR benefits from spatially cleaned beams, the CHARA Classic beam combiner has greater sensitivity. Hence, the two instruments complement each other in this respect.

The same near-IR detector was at the back end of each beam combiner. The fringe sampling frequency was either 100 or 150 Hz, depending on the seeing conditions and source brightness. For the same reasons, either 1 or 2 × 2 pixels were read out. The camera readout was adjusted to maintain five samples per fringe. Each merged data scan from CHARA Classic was formed from 200 scans with photometric calibration scans made before and after. Photometric calibration scans for FLUOR are performed during the scan on separate fiber channels.

Atmospheric and instrumental coherence losses were estimated by interleaving measurements of unresolved stars or stars with known angular diameters. Calibrators were chosen using the *gcWeb* utility available online from the Michelson Science Center.[3] We restricted our selection to main-sequence stars with estimated angular sizes less than 0.4 mas, which yields visibility amplitudes greater than 90% when measured with the S1-E1 baseline in the K' band. The calibrator observations were in close proximity on the sky (within 10°) and in time (within 30 minutes) to each source observation. The typical duty cycle from the start

---

[2] See http://vizier.hia.nrc.ca/viz-bin/Cat?J/A%2bA/433/1155.
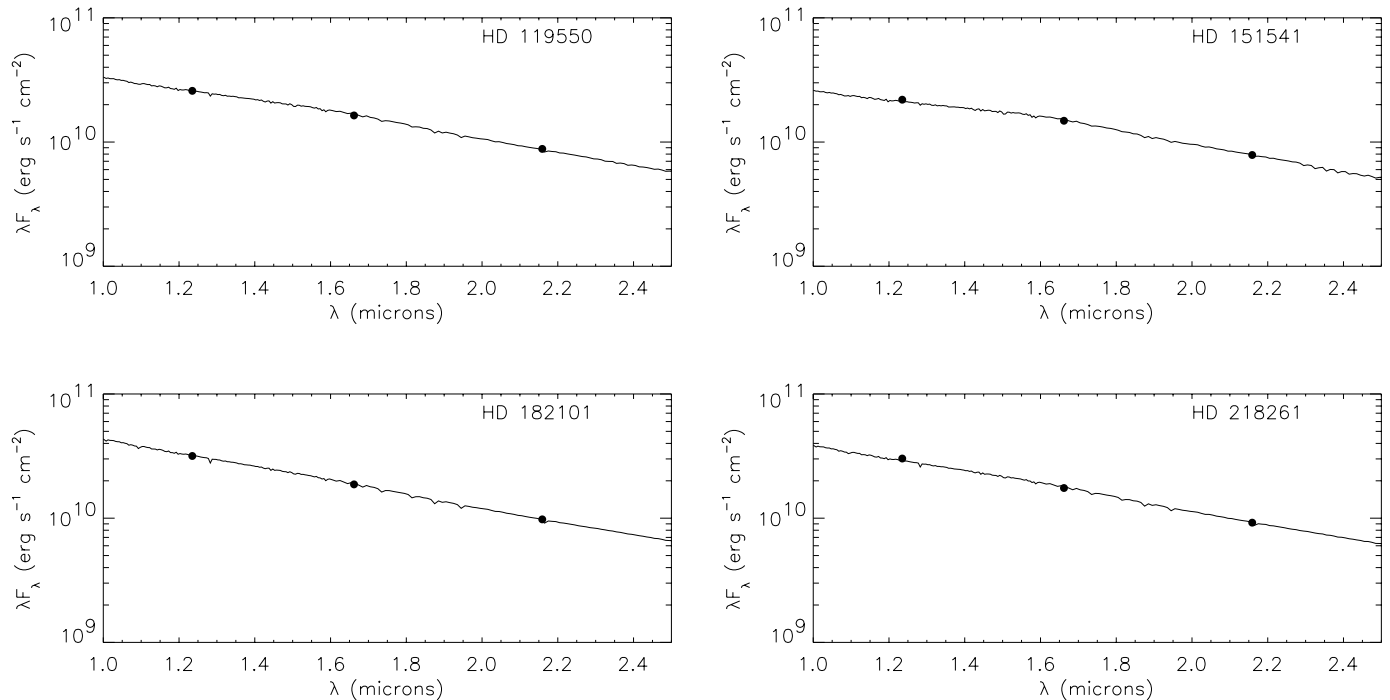[3] See http://mscweb.ipac.caltech.edu/gcWeb/gcWeb.jsp.

FIG. 1.— Spectral energy distribution fits used to derive the calibrator angular diameters from the IRF method. The model atmosphere fluxes (Kurucz 1992) are shown as a solid line, and the filled circles give the observed fluxes from the 2MASS *J, H, K* photometry (Cutri et al. 2003; Cohen et al. 2003). The errors in the 2MASS fluxes are approximately ±2% (much smaller than the symbol size).

of one observation to the start of the next was approximately 10 minutes.

3. DATA REDUCTION

The reduction algorithms developed for data from the CHARA Array are described in detail by ten Brummelaar et al. (2005). We employed a commonly used technique of integrating the power of each fringe scan (Benson et al. 1995), but we removed the variance term resulting from atmospheric turbulence. The resulting quantity is the visibility amplitude ($\mathcal{V}$) and not the more common $\mathcal{V}^2$. Data from GJ 15A and its calibrator were analyzed by methods specific to the FLUOR instrument (Coudé du Foresto et al. 1997; Perrin 2003), and the following description does not pertain.

The calibrated visibility amplitude of the science object ($\mathcal{V}_o$) was calculated using the relation

$$\mathcal{V}_o = \frac{1}{\eta} \mathcal{V}'_o, \qquad (1)$$

where η is the interferometer's efficiency and $\mathcal{V}'_o$ is the instrumental visibility amplitude of the science object as measured on the sky. By interleaving measurements of a calibrator of known angular size and thus a known calibrated visibility amplitude, one can measure η via the ratio of the instrumental to calibrated visibility amplitude, or $\eta = \mathcal{V}'_c/\mathcal{V}_c$. Furthermore, if the calibrator is unresolved, $\mathcal{V}_c$ is unity and η is measured directly. However, the high resolution at long baselines and instrument sensitivity limitations significantly reduce the number of available unresolved sources, especially within close proximity to the science object. Therefore, we were left to use slightly resolved calibrators and to determine $\mathcal{V}_c$ through other means.

3.1. *Angular Diameters of the Calibrators*

From conservation of energy, the true limb-darkened angular diameter of a star (θ_{LD}) is related to the ratio of the stellar flux reaching the top of the Earth's atmosphere ($F_\lambda^\oplus$) at wavelength λ to the flux leaving the stellar surface ($F_\lambda^\star$):

$$\frac{\theta_{LD}^2}{4} = \frac{F_\lambda^\oplus}{F_\lambda^\star}. \qquad (2)$$

Here $F_\lambda^\star$ is determined from stellar model atmospheres and $F_\lambda^\oplus$ from extinction-corrected photometry and absolute spectrophotometry. This was an idea first proposed by Gray (1967) and later refined by Blackwell & Shallis (1977). A potential source of error in $F_\lambda^\star$ is the uncertainty in determining the correct input parameters for the model atmosphere. For example, if the effective temperature ($T_{\rm eff}$), metallicity ([Fe/H]), and/or surface gravity (log g) are not well known, there can be difficulty in choosing the correct model. As pointed out by Blackwell & Shallis, the infrared region is less sensitive to model input approximations than the visible— hence the method to derive angular diameters from infrared photometry is known as the infrared flux (IRF) method. Because our observations were obtained in the K' band, our derived radius measurements are relatively unaffected by problems related to limb darkening and/or absorption line contamination.

We selected model atmospheres from Kurucz (1992) and linearly interpolated the fluxes between $T_{\rm eff}$ grid points. We adopted log g = 4.5, which is appropriate for midtemperature dwarf stars, and assumed the metallicity to be solar. However, changing log g and/or the metallicity did not significantly effect the resulting θ_{LD}. The Two Micron All Sky Survey (2MASS) point source catalog (Cutri et al. 2003) provided the near-IR broadband photometry data, which were then transformed to fluxes (Cohen et al. 2003). A weighted fit of the 2MASS photometry to the model flux yielded angular diameters less than 0.4 mas and typical errors of 4%–5% (Fig. 1). For calibrators with such small angular size, the propagated fractional error in the target angular diameter is much lower than this percentage (van Belle & van Belle 2005).

TABLE 2
CALIBRATORS

HD Number (1)	Spectral Classification (2)	$\log(T_{\rm eff})^{\rm a}$ (K) (3)	$[{\rm Fe/H}]^{\rm a}$ (4)	$\theta_{\rm LD}$ (mas) (5)	ρ_w (6)	$\theta_{\rm UD}$ (mas) (7)
119550............	G2 V[b]	3.755	−0.07	0.363 ± 0.015	1.0148	0.358 ± 0.015
151541............	K1 V[c]	3.719	−0.36	0.326 ± 0.013	1.0165	0.321 ± 0.013
182101............	F6 V[d]	3.799	−0.42	0.367 ± 0.017	1.0120	0.363 ± 0.017
218261............	F8.5 V[e]	3.799	0.00	0.387 ± 0.021	1.0139	0.382 ± 0.021

[a] Nordstrom et al. (2004).
[b] Harlan (1969).
[c] Cowley et al. (1967).
[d] Bidelman (1957).
[e] Gray et al. (2001).

We list the names and adopted parameters of the calibrator stars in Table 2, and our derived $\theta_{\rm LD}$ values are given there in column (5).

The IRF method yields $\theta_{\rm LD}$. However, it is common practice to fit a visibility function for a uniform disk angular diameter ($\theta_{\rm UD}$), which is given by

$$\mathcal{V} = \left| \frac{2 J_1(\pi B \theta_{\rm UD}/\lambda_0)}{\pi B \theta_{\rm UD}/\lambda_0} \right| \qquad (3)$$

and depends on the projected baseline (B) and the effective wavelength (λ_0). In order to compute the efficiency (η) from the measured visibility of the calibrator ($\mathcal{V}'_c$), we need to transform $\theta_{\rm LD}$ into an equivalent $\theta_{\rm UD}$ that has the same visibility amplitude at the observed projected baseline and wavelength. To do this, we calculated a correction factor ($\rho_w = \theta_{\rm LD}/\theta_{\rm UD}$) based on $T_{\rm eff}$, metallicity (Nordstrom et al. 2004), and the transmission of the K' filter (Davis et al. 2000; Tango & Davis 2002). These correction factors (Table 2, col. [6]) result in slightly smaller ($\approx$1.5%) diameters for equivalent uniform disks.

3.2. Calibrated Visibility Amplitudes

Because calibrator measurements were not made simultaneously with object measurements, we linearly interpolated between the values of $\mathcal{V}'_c$ immediately before and after each $\mathcal{V}'_o$. We then used the calibrator $\theta_{\rm UD}$ and the known values of B and λ_0 to compute $\mathcal{V}_c$. From $\mathcal{V}'_c$ and $\mathcal{V}_c$ we determined the instrumental efficiency (η) for visibility measurement. Typically, values of η ranged from 40% to 50% and varied by only a few percent over the course of the night. This can be attributed to the stability of the system and habitual realignment of the optics before every observation. Finally, from equation (1), we determined the calibrated visibility amplitudes ($\mathcal{V}_o$). Table 3 lists the modified Julian dates (MJD), projected baselines, and visibility amplitudes (with error estimates) associated with the midpoint time of observation for each dwarf star. Errors in calibrator angular size (§ 3.1) and visibility amplitudes were propagated to the calibrated visibility amplitude error estimates.

4. ANGULAR DIAMETERS AND RADII

We can determine the stellar radius from the angular diameter and parallax in two ways. First, we can assume that the stars are uniform disks and then fit the fringe visibility as a function of baseline using equation (3). This estimate of $\theta_{\rm UD}$ is given in column (2) of Table 4. However, we know that real stars are limb-darkened (by a small amount in the K' band), so that their actual, limb-darkened diameters will be slightly larger than the uniform disk diameters (see Table 2). In principle, it is no harder to fit a limb-darkened visibility curve to the observations (Davis et al. 2000, eq. [6]), but to do so we first need to establish the stellar parameters in order to obtain the appropriate K'-band limb-darkening law from stellar atmosphere models.

We approached this problem as follows. Claret (2000) has tabulated limb-darkening coefficients for the near-IR that are based on solar metallicities. We chose the coefficients calculated using the PHOENIX code for modeling stellar atmospheres (Claret 2000, Table 38). The limb-darkening relations are listed as functions of $T_{\rm eff}$ and $\log g$. We can determine these parameters using an iterative scheme that is based on sequential improvements in the radius estimate. We start with a stellar radius estimate derived from the uniform disk angular diameter (Table 4, col. [2]) and the parallax from the NStars database.[4] NStars parallaxes are the weighted means of all currently available parallaxes, including those of *Hipparcos* and the Yale Parallax Catalog. Then we use the Stefan-Boltzmann relation to find $T_{\rm eff}$ from the bolometric luminosity and radius. We determined the bolometric luminosity from the absolute K magnitude using a bolometric correction based on the $I - K$ color index (derived from spectral energy distribution fits of M stars by Leggett et al. 2000). We used absolute K magnitudes calculated from NStars parallaxes and 2MASS K magnitudes and $I - K$ color indices from Leggett (1992) to find the luminosities given in column (5) of Table 4, which were then used to find $T_{\rm eff}$ from the assumed stellar radius. We adopted $L_\odot = 3.86 \times 10^{33}$ ergs s^{-1} and $M_{\rm bol\odot} = 4.75$ in this calculation, and the scatter in the bolometric correction relation results in a luminosity error of ± 0.022 dex. Next we used estimates of the stellar mass (col. [4] of Table 5) with the assumed radius to find $\log g$. Stellar masses were estimated using the K-band mass-luminosity relation of Delfosse et al. (2000), which have a typical error of $\pm 10\%$. With $T_{\rm eff}$ and $\log g$ set, we then found the limb-darkening law from Claret (2000) and made a least-squares error-weighted fit of the limb-darkened visibility curve to the observations to obtain the limb-darkened angular size $\theta_{\rm LD}$.

We repeated the process and revised the temperature and gravity estimates by estimating a new radius from $\theta_{\rm LD}$ and parallax and then fitted the visibilities again with the revised limb-darkened visibility curve. In practice, this procedure converged (with negligible parameter differences between iterations) in

---

[4] See http://nstars.nau.edu.

TABLE 3
Calibrated K' Visibilities

Object Name	Date (MJD)	Baseline (m)	Visibility
GJ 15A............................	53,287.364	304.7	0.290 ± 0.013[a]
	53,287.390	296.8	0.305 ± 0.021[a]
GJ 514............................	53,167.188	298.3	0.716 ± 0.042
	53,167.230	287.8	0.643 ± 0.038
	53,167.259	284.8	0.697 ± 0.037
	53,167.279	285.0	0.734 ± 0.046
	53,168.188	297.4	0.731 ± 0.039
	53,168.210	291.4	0.727 ± 0.035
	53,168.234	286.7	0.756 ± 0.037
	53,168.255	284.8	0.845 ± 0.042
	53,170.185	296.7	0.722 ± 0.030
	53,170.204	291.5	0.652 ± 0.030
	53,170.224	287.5	0.730 ± 0.033
	53,170.243	285.2	0.854 ± 0.042
	53,170.265	284.7	0.801 ± 0.038
	53,170.285	286.4	0.801 ± 0.045
GJ 526............................	53,162.272	297.7	0.688 ± 0.043
	53,162.291	297.0	0.702 ± 0.043
	53,162.313	298.0	0.672 ± 0.039
	53,163.245	300.7	0.645 ± 0.036
	53,164.224	304.1	0.569 ± 0.031
	53,169.180	311.4	0.555 ± 0.024
	53,169.201	306.1	0.637 ± 0.026
	53,169.241	298.9	0.734 ± 0.035
	53,169.259	297.3	0.734 ± 0.030
	53,169.278	297.0	0.691 ± 0.028
GJ 687............................	53,182.186	253.3	0.727 ± 0.041
	53,182.200	258.8	0.715 ± 0.044
	53,182.213	263.7	0.644 ± 0.041
	53,182.227	268.4	0.578 ± 0.035
	53,182.241	272.5	0.535 ± 0.033
GJ 752A........................	53,161.452	282.4	0.779 ± 0.040
	53,161.470	276.5	0.735 ± 0.036
	53,162.405	300.2	0.638 ± 0.041
	53,162.433	288.5	0.641 ± 0.035
	53,162.449	282.3	0.662 ± 0.041
	53,162.468	276.2	0.664 ± 0.042
	53,164.449	280.6	0.694 ± 0.044
	53,164.462	276.4	0.650 ± 0.042
	53,167.359	312.9	0.713 ± 0.043
	53,167.376	306.6	0.618 ± 0.035
	53,167.391	300.1	0.711 ± 0.038
	53,167.411	291.9	0.704 ± 0.043
	53,167.424	286.8	0.680 ± 0.052
	53,167.437	281.8	0.726 ± 0.053
	53,167.457	275.4	0.713 ± 0.047
	53,168.332	321.3	0.599 ± 0.063
	53,168.400	295.2	0.650 ± 0.042
	53,168.421	286.8	0.751 ± 0.056
	53,169.313	325.4	0.580 ± 0.030
	53,169.326	322.1	0.609 ± 0.035
	53,169.339	318.0	0.503 ± 0.032
	53,169.352	313.7	0.635 ± 0.040
	53,169.366	308.3	0.666 ± 0.041
	53,169.381	301.9	0.572 ± 0.040
	53,169.396	295.7	0.692 ± 0.041
	53,169.410	290.2	0.689 ± 0.040
	53,169.424	284.7	0.731 ± 0.042
	53,169.436	280.3	0.649 ± 0.043
	53,170.322	322.4	0.646 ± 0.033
	53,170.338	317.7	0.672 ± 0.034
	53,170.352	312.7	0.628 ± 0.032
	53,170.372	304.9	0.662 ± 0.032
	53,170.384	299.7	0.760 ± 0.040

TABLE 3— *Continued*

Object Name	Date (MJD)	Baseline (m)	Visibility
	53,170.399	293.6	0.629 ± 0.039
	53,170.412	288.1	0.682 ± 0.044
	53,170.425	283.3	0.734 ± 0.044
GJ 880............................	52,928.301	247.4	0.727 ± 0.024
	52,928.315	244.7	0.716 ± 0.026
	52,928.326	241.7	0.731 ± 0.024
	52,928.334	238.9	0.718 ± 0.022
	52,928.351	231.7	0.698 ± 0.025

[a] Visibilities are given as $\mathcal{V}^2$.

only two iterations because the IR limb darkening is only slightly different from a uniform disk and is relatively insensitive to the adopted temperature and gravity. In fact, a 1 σ change in the adopted temperature and gravity has no detectable effect on θ_{LD}. Our final values of θ_{LD}, reduced χ^2 (χ^2_{red}), stellar radius, T_{eff}, and log g are listed in Table 4, and the fitted, limb-darkened visibility curves are plotted with the observations in Figure 2. The fractional errors in the derived temperatures are approximately one-half the fractional errors in the radii or about 3%, and the errors in log g amount to approximately ±0.07 dex (as derived from the errors in fractional mass and radius). Changing these parameters by 1 standard deviation does not effect the radius determinations at the precision we are reporting them.

The one inconsistency in this method is that we have relied on the solar abundance atmospheric models from Claret (2000) to estimate the limb darkening, while some of our targets are somewhat metal-poor (Table 5, col. [3]). It will be interesting to revisit our calculations when limb-darkening results for metal-poor atmospheres are eventually developed, but we doubt that our radius results will change significantly because the limb-darkening corrections are small.

We found that the values of χ^2_{red} (given in Table 4, col. [4]) exceeded the expected value of unity for all the targets except GJ 15A and GJ 880 (the small value for GJ 15A probably results from our sample of two measurements). Thus, the internal visibility amplitude errors associated with an individual data set underestimate the full error budget, and consequently, we used the observed scatter from the fits to rescale the minimum best-fit value of χ^2_{red} to unity. We added a 6% noise floor to account for the night-to-night fluctuation in angular diameter measurement, as calculated from objects with multinight observations. This term was added in quadrature to the statistical error. We show in Figure 3 the distribution of the fractional deviations from the fit for GJ 752A, the target with the most observations. We also plot a linear regression fit of the residuals, which has a nonzero slope that is set by a few outlying points from two nights (2004 June 13–14). The 6% noise floor also accounts for this slight linear trend seen in these commissioning observations.

We also determined effective temperatures by a direct comparison of the observed and predicted fluxes in the K band based on the observed angular diameters. We used the 2MASS K_s-band magnitudes and the adopted flux zero point from Cohen et al. (2003) to form the following relation:

$$K_s = -2.5 \log F_\lambda - 5 \log \theta_{LD} + 17.157, \qquad (4)$$

where F_λ is the model flux (ergs cm^{-2} s^{-1} Å^{-1}) averaged over the 2MASS K_s-filter response (Cohen et al. 2003) and θ_{LD} is the

TABLE 4
Derived Stellar Parameters

Object Name (1)	θ_{UD} (mas) (2)	θ_{LD} (mas) (3)	χ^2_{red} (4)	$\log L_{\mathrm{bol}}$ (ergs s^{-1}) (5)	Radius ($R_{\odot}$) (6)	T_{eff}(BC) (K) (7)	T_{eff}(2MASS) (K) (8)	$\log g$ (cm s^{-2}) (9)
GJ 15A..............	0.976 ± 0.016	0.988 ± 0.016	0.06	31.99	0.379 ± 0.006	3747	3730 ± 49	4.89
GJ 514...............	0.740 ± 0.044	0.753 ± 0.052	2.50	32.22	0.611 ± 0.043	3377	3243 ± 160	4.59
GJ 526...............	0.830 ± 0.050	0.845 ± 0.057	3.41	32.18	0.493 ± 0.033	3662	3636 ± 163	4.75
GJ 687...............	0.990 ± 0.059	1.009 ± 0.077	3.06	31.91	0.492 ± 0.038	3142	3095 ± 107	4.66
GJ 752A............	0.822 ± 0.049	0.836 ± 0.051	1.49	32.10	0.526 ± 0.032	3390	3368 ± 137	4.68
GJ 880...............	0.918 ± 0.055	0.934 ± 0.059	0.92	32.32	0.689 ± 0.044	3373	3277 ± 93	4.53

limb-darkened angular diameter (mas). The model fluxes were taken from the PHOENIX atmosphere code of Brott & Hauschildt (2005),[5] and these are primarily functions of effective temperature (although we did interpolate in these models for the appropriate gravity and metallicity of each target). We used our values of θ_{LD} from Table 4 to find the estimates of $F_{\lambda}(T_{\mathrm{eff}})$ and hence effective temperature that are listed in column (8) of Table 4 [under the heading T_{eff}(2MASS)]. The temperatures agree well with those from the bolometric correction method, T_{eff}(BC), discussed above. Note that the adopted limb-darkened diameters themselves depend on the assumed temperature through the limb-darkening coefficients, but since the resulting temperatures are so similar and the limb darkening is a minor effect, this approximation has a negligible impact on the temperature derived this way.

Finally, we note that we find no evidence in our data that any target has a close binary companion that could affect the radius estimates. The targets are all radial velocity constant (rms <100 m s^{-1}) according to the spectroscopic survey of Nidever et al. (2002). Optical speckle interferometry by McAlister et al. (1987) and Balega et al. (1999) indicates that GJ 687 has a companion at a separation of 0″3, which is too wide to influence our observations (except as a source of incoherent light that might reduce the measured visibility). However, near-infrared speckle observations (Leinert et al. 1997) and high-resolution *HST* NICMOS imaging (T. J. Henry 2006, private communication) show no evidence of a companion at such a separation. We examined the mean fringe envelopes for each set of scans of this star and found no detectable companion with $\Delta K_s < 2$ in the separation range 12–70 mas. Clearly, more observations are

[5] See ftp://ftp.hs.uni-hamburg.de/pub/outgoing/phoenix/GAIA.

TABLE 5
Adopted Stellar Parameters

Object Name (1)	Spectral Classification[a] (2)	[Fe/H][b] (3)	Mass[c] ($\mathcal{M}_{\odot}$) (4)	Parallax[d] (arcsec) (5)
GJ 15A...................	M1.5 V	-0.46	0.404	0.28059 ± 0.00095
GJ 514...................	M1.0 V	-0.27	0.526	0.13257 ± 0.00118
GJ 526...................	M1.5 V	-0.31	0.502	0.18421 ± 0.00116
GJ 687...................	M3.0 V	$+0.11$	0.401	0.22049 ± 0.00082
GJ 752A................	M3.0 V	-0.05	0.484	0.17101 ± 0.00062
GJ 880...................	M1.5 V	-0.04	0.586	0.14579 ± 0.00113

[a] From Henry et al. (1994).
[b] From Bonfils et al. (2005). The typical error in [Fe/H] is ± 0.2 dex.
[c] From Delfosse et al. (2000) and we adopted a 10% error in mass.
[d] NStars database, http://nstars.nau.edu.

required to settle the question about a companion to GJ 687, but we tentatively assume that the measured visibility is dominated by the photospheric disk of the bright M dwarf.

5. MASS-RADIUS RELATION

In an effort to further constrain the poorly populated mass-radius relation for low-mass stars, we started by comparing our results with other low-mass stellar radii directly measured with long-baseline interferometers (Lane et al. 2001; Ségransan et al. 2003). All masses were derived from the same K-band mass-luminosity relation of Delfosse et al. (2000), and we adopted a 10% error to account for photometric and empirical fitting errors. Note that the mass derived from the absolute K magnitude should have little or no dependence on the stellar metallicity (Baraffe et al. 1998, see Fig. 3b). Lane et al. (2001) also measured the angular diameter of GJ 15A, and their value of $\theta_{\mathrm{UD}} = 0.985 \pm 0.05$ mas agrees with our value $\theta_{\mathrm{UD}} = 0.976 \pm 0.016$ mas. However, we adopted a less severe limb-darkening correction resulting in a smaller linear diameter. In our mass-radius plot (Fig. 4), we only show our data point for GJ 15A. Eclipsing binary star measurements are also shown in Figure 4 as open circles, and it should be noted that some of the errors bars are smaller than the symbol size. The theoretical models of Chabrier & Baraffe (1997) for [M/H] = 0, -0.5, and -1.0 are shown as the lines. In addition, the models of Siess et al. (1997) for [M/H] = 0, -0.3 (assuming $Z_{\odot} = 0.02$) are plotted to show the range of model uncertainty. According to these models, metallicity should have little effect on radius for a given mass star. However, there is either a systematic effect in the data or the models are underestimating the sizes of the stars for a given mass. We doubt the former possibility because this effect is seen in data from multiple instruments and is present in both the interferometric and binary results. Indeed, the larger than expected radii have already been noted in several investigations (Leggett et al. 2000; Ségransan et al. 2003; López-Morales & Ribas 2005).

Mullan & MacDonald (2001) argue that larger radii could result from pervasive magnetic fields that could alter the interior structure and push the occurrence of completely convective interiors to stars of lower effective temperatures. They suggest that M stars with active magnetic fields will have larger radii than those predicted by standard models. However, there is no evidence that the M dwarfs in our sample have any special magnetic properties. All are slow rotators (Delfosse et al. 1998), have moderate X-ray coronal emission (Schmitt et al. 1995; Hünsch et al. 1999), have normal chromospheric Hα lines (Gizis et al. 2002), and show no evidence of photometric variability in *Hipparcos* photometry (Perryman et al. 1997). Thus, these stars do not have the exceptionally strong magnetic fields
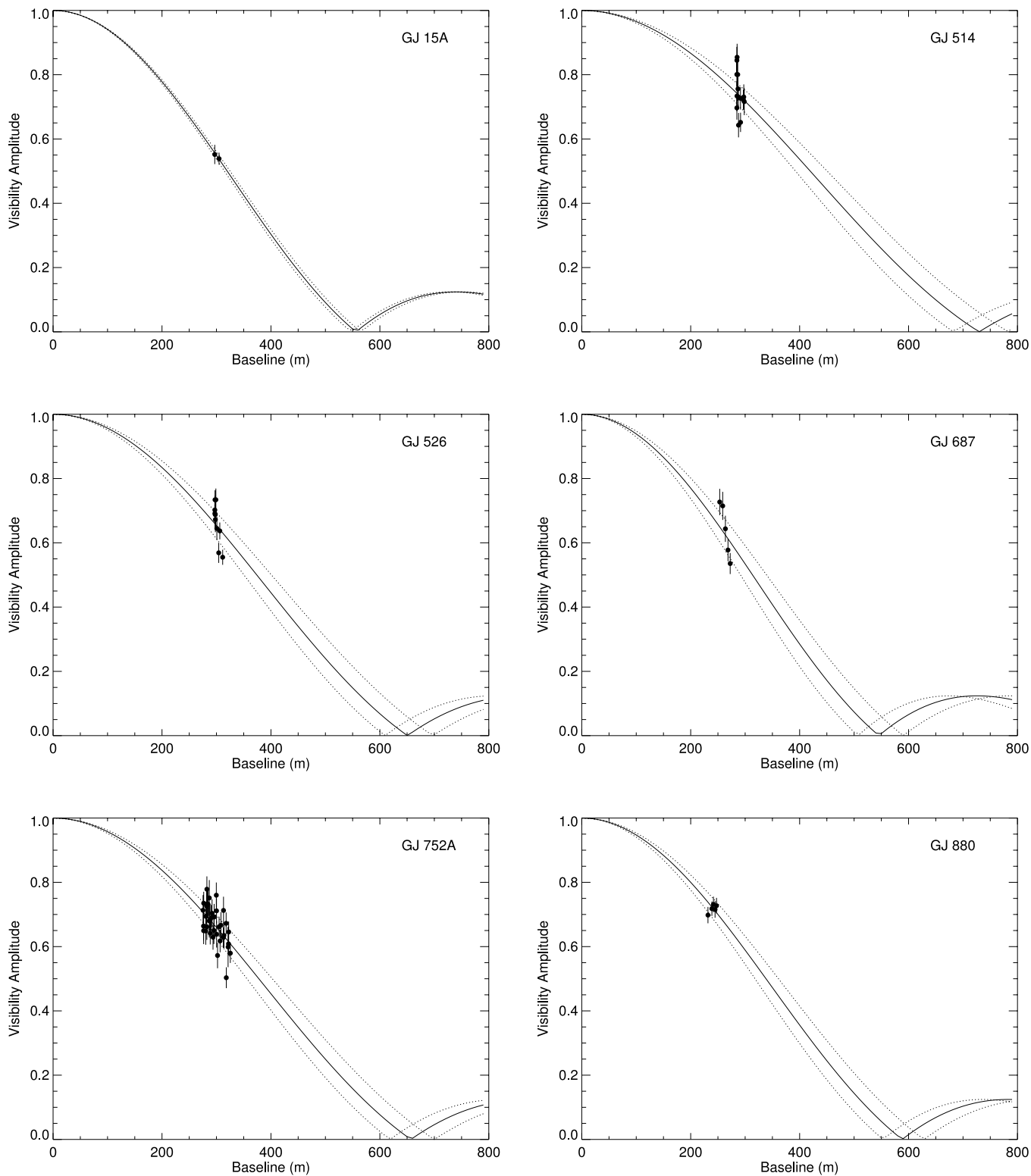
FIG. 2.—Observed visibilities and fitted visibility curve (*solid line*) for a limb-darkened disk (using a *K*-band limb darkening law from Claret [2000] for the stellar parameters given in Table 4). Dotted lines represent the total error to the model fit.
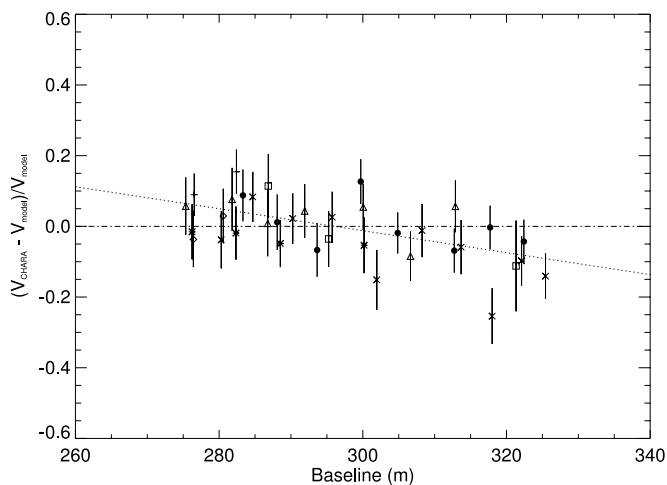
FIG. 3.—Fractional deviation between the observed visibilities and fitted visibility curve for a limb-darkened disk (same as in Fig. 2) for GJ 752A. The dotted line represents a best-fit regression line. Symbols indicated data taken on different nights (*plus signs*: 2004 June 5; *asterisks*: 2004 June 6; *diamonds*: 2004 June 8; *triangles*: 2004 June 11; *squares*: 2004 June 12; *crosses*: 2004 June 13; *circles*: 2004 June 14).
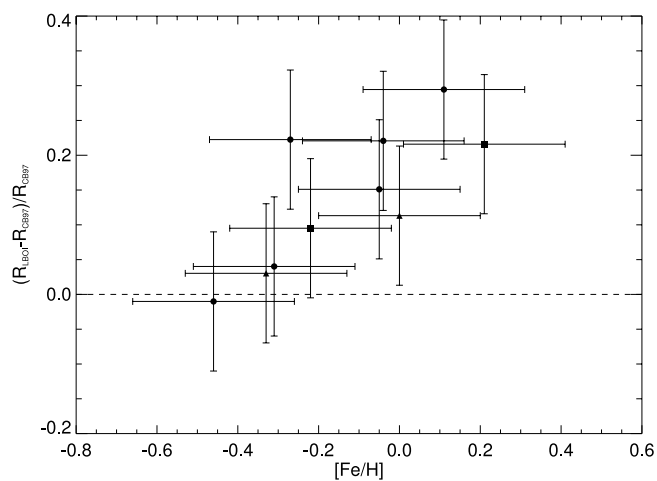

FIG. 5.—Fractional deviation between the radii measured through long baseline optical interferometry (R_{LBOI}) and from the model predictions for stellar radius from Chabrier & Baraffe (1997; R_{CB97}) plotted as a function of metallicity. The symbols represent the same observational groups given in Fig. 4. The representative errors are ± 0.2 dex in [Fe/H] and ± 0.1 in fractional deviation of the radius (due to 10% errors in the mass estimates).

that would lead to larger radii according to the models of Mullan & MacDonald.

On the other hand, our sample stars do span a significant range in metallicity, and metallicity will play a role in the internal structure of M stars. To investigate this possibility, we plot in Figure 5 the fractional deviation from the [M/H] = 0 model prediction as a function of metallicity. The metallicities for most stars are taken from Bonfils et al. (2005) except for those of GJ 191, GJ 205, GJ 887 (Woolf & Wallerstein 2005), and GJ 699 (Kotoneva et al. 2005). Efforts to derive accurate metallicities for M dwarfs are in the nascent phase at this time, so the metallicity values should be considered preliminary, although the general trends

are likely reliable. We see that the observed radii are approximately consistent with predictions among the metal-poor stars, but the radii become larger than predicted as the metallicity increases. The same conclusion can be drawn from the results of Leggett et al. (2000), who show that the radii derived from spectral fits are systematically larger among stars with higher metallicity when plotted in a (T_{eff}, R) diagram (see their Fig. 13). Because metallicity is closely related to stellar opacity, we suspect that the current generation of models for the interiors and atmospheres of M stars is missing some opacity component that results in larger radii for stars of higher metallicity. We are planning to expand this investigation to other targets with a wider range in metallicity in order to explore this connection further. This work will include more spatial coverage via different baselines and observations at shorter wavelengths to obtain measurements farther along the visibility curves.

FIG. 4.—Mass-radius relation for low-mass dwarfs measured by long-baseline interferometry (*filled symbols*) and spectrophotometry of eclipsing binaries (*open circles*; see references in § 1). The interferometry data included are from this paper (*circles*), PTI (Lane et al. 2001, *triangles*), and VLTI (Ségransan et al. 2003, *squares*). The lines represent models from Chabrier & Baraffe (1997) for different metallicities (*dotted line*: [M/H]= 0.0; *short-dashed line*: [M/H]= −0.5; *double-dot-dashed line*: [M/H]= −1.0) and Siess et al. (1997) for similar metallicities (*solid line*: [M/H]= 0.0; *long-dashed line*: [M/H]= −0.3).

REFERENCES

Andersen, J. 1991, Astron. Astrophys. Rev., 3, 91
Balega, I. I., Balega, Y. Y., Maksimov, A. F., Pluzhnik, E. A., Shkhagosheva, Z. U., & Vasyuk, V. A. 1999, A&AS, 140, 287
Baraffe, I., Chabrier, G., Allard, F., & Hauschildt, P. H. 1998, A&A, 337, 403
Benson, J. A., Dyck, H. M., & Howell, R. R. 1995, Appl. Opt., 34, 51
Bidelman, W. P. 1957, PASP, 69, 147
Blackwell, D. E., & Shallis, M. J. 1977, MNRAS, 180, 177
Bonfils, X., Delfosse, X., Udry, S., Santos, N. C., Forveille, T., & Ségransan, D. 2005, A&A, 442, 635
Brott, I., & Hauschildt, P. H. 2005, in The Three-dimensional Universe with Gaia, ed. C. Turon, K. S. O'Flaherty, & M. A. C. Perryman (ESA SP-576; Noordwijk: ESA), 565
Chabrier, G., & Baraffe, I. 1997, A&A, 327, 1039
Claret, A. 2000, A&A, 363, 1081
Cohen, M., Wheaton, W. A., & Megeath, S. T. 2003, AJ, 126, 1090
Costa, E., Méndez, R. A., Jao, W.-C., Henry, T. J., Subasavage, J. P., Brown, M. A., Ianna, P. A., & Bartlett, J. 2005, AJ, 130, 337
Coudé du Foresto, V., Ridgway, S., & Mariotti, J.-M. 1997, A&AS, 121, 379
Coudé du Foresto, V., et al. 2003, Proc. SPIE, 4838, 280
Cowley, A. P., Hiltner, W. A., & Witt, A. N. 1967, AJ, 72, 1334
Creevey, O. L., et al. 2005, ApJ, 625, L127
Cutri, R. M., et al. 2003, The 2MASS All-Sky Catalog of Point Sources (Pasadena: IPAC)
Davis, J., Tango, W. J., & Booth, A. J. 2000, MNRAS, 318, 387
Delfosse, X., Forveille, T., Perrier, C., & Mayor, M. 1998, A&A, 331, 581
Delfosse, X., Forveille, T., Ségransan, D., Beuzit, J.-L., Udry, S., Perrier, C., & Mayor, M. 2000, A&A, 364, 217
Gizis, J. E., Reid, I. N., & Hawley, S. L. 2002, AJ, 123, 3356
Gliese, W., & Jahreiß, H. 1991, Preliminary Version of the Third Catalogue of Nearby Stars (Greenbelt: NASA)
Gray, D. F. 1967, ApJ, 149, 317
Gray, R. O., Napier, M. G., & Winkler, L. I. 2001, AJ, 121, 2148
Hambly, N. C., Henry, T. J., Subasavage, J. P., Brown, M. A., & Jao, W.-C. 2004, AJ, 128, 437
Harlan, E. A. 1969, AJ, 74, 916
Henry, T. J., Ianna, P. A., Kirkpatrick, J. D., & Jahreiss, H. 1997, AJ, 114, 388
Henry, T. J., Kirkpatrick, J. D., & Simons, D. A. 1994, AJ, 108, 1437
Hünsch, M., Schmitt, J. H. M. M., Sterzik, M. F., & Voges, W. 1999, A&AS, 135, 319
Jao, W.-C., Henry, T. J., Subasavage, J. P., Brown, M. A., Ianna, P. A., Bartlett, J. L., Costa, E., & Méndez, R. A. 2005, AJ, 129, 1954
Kotoneva, E., Innanen, K., Dawson, P. C., Wood, P. K., & de Robertis, M. M. 2005, A&A, 438, 957

Kurucz, R. L. 1992, in Proc. IAU Symp. 149, The Stellar Populations of Galaxies, ed. B. Barbuy & A. Renzini (Dordrecht: Kluwer), 225
Lacy, C. H. 1977, ApJ, 218, 444
Lane, B. F., Boden, A. F., & Kulkarni, S. R. 2001, ApJ, 551, L81
Leggett, S. K. 1992, ApJS, 82, 351
Leggett, S. K., Allard, F., Dahn, C., Hauschildt, P. H., Kerr, T. H., & Rayner, J. 2000, ApJ, 535, 965
Leinert, C., Henry, T., Glindemann, A., & McCarthy, D. W. 1997, A&A, 325, 159
Lépine, S. 2005, AJ, 130, 1680
López-Morales, M., & Ribas, I. 2005, ApJ, 631, 1120
Luyten, W. J. 1979, LHS Catalogue: A Catalogue of Stars with Proper Motions Exceeding 0″.5 Annually (2nd ed.; Minneapolis: Univ. Minnesota)
Maceroni, C., & Montalbán, J. 2004, A&A, 426, 577
Maxted, P. F. L., Marsh, T. R., Morales-Rueda, L., Barstow, M. A., Dobbie, P. D., Schreiber, M. R., Dhillon, V. S., & Brinkworth, C. S. 2004, MNRAS, 355, 1143
McAlister, H. A., Hartkopf, W. I., Hutter, D. J., & Franz, O. G. 1987, AJ, 93, 688
McAlister, H. A., et al. 2005, ApJ, 628, 439
Mérand, A., Bordé, P., & Coudé du Foresto, V. 2005, A&A, 433, 1155
Metcalfe, T. S., Mathieu, R. D., Latham, D. W., & Torres, G. 1996, ApJ, 456, 356
Mullan, D. J., & MacDonald, J. 2001, ApJ, 559, 353
Nidever, D. L., Marcy, G. W., Butler, R. P., Fischer, D. A., & Vogt, S. S. 2002, ApJS, 141, 503
Nordstrom, B., et al. 2004, A&A, 418, 989
Ochsenbein, F., Bauer, P., & Marcout, J. 2000, A&AS, 143, 23
Perrin, G. 2003, A&A, 400, 1173
Perryman, M. A. C., et al. 1997, A&A, 323, L49
Reid, I. N., et al. 2004, AJ, 128, 463
Ribas, I. 2003, A&A, 398, 239
Schmitt, J. H. M. M., Fleming, T. A., & Giampapa, M. S. 1995, ApJ, 450, 392
Ségransan, D., Kervella, P., Forveille, T., & Queloz, D. 2003, A&A, 397, L5
Siess, L., Forestini, M., & Dougados, C. 1997, A&A, 324, 556
Sturmann, J., ten Brummelaar, T. A., Ridgway, S. T., Shure, M. A., Safizadeh, N., Sturmann, L., Turner, N. H., & McAlister, H. A. 2003, Proc. SPIE, 4838, 1208
Subasavage, J. P., Henry, T. J., Hambly, N. C., Brown, M. A., Jao, W.-C., & Finch, C. T. 2005, AJ, 130, 1658
Tango, W. J., & Davis, J. 2002, MNRAS, 333, 642
ten Brummelaar, T. A., et al. 2005, ApJ, 628, 453
Torres, G., & Ribas, I. 2002, ApJ, 567, 1140
van Belle, G. T., & van Belle, G. 2005, PASP, 117, 1263
van Belle, G. T., et al. 2006, ApJ, 637, 494
Woolf, V. M., & Wallerstein, G. 2005, MNRAS, 356, 963